ISME

Iranian Journal of Mechanical Engineering
The Iranian Society of Mechanical Engineers
Research Paper
DOI: 10.30506/jmee.2021.129082.1234

Capturing of Shock Wave of Supersonic Flow Over the Bump Channel with TVD, ACM and Jameson Methods

M.Yadegari[*]
PhD

M.A. Jahdi[†]
Assistant Professor

The phenomenon of capturing of sharp gradients, shock waves, and contact discontinuities in compressible aerodynamic flows is the major concern while numerical methods based on the characteristic variables are favorable solutions. The aim of the present study is to introduce a method based on the characteristic variables (Riemann solution) and control the diffusion term in the classic methods in order to capture the shock waves. An efficient blending procedure based on the density-based algorithm is presented to solve the compressible Euler equations, using a non-orthogonal mesh with collocated finite volume formulation. The fluxes of the convected quantities are approximated by employing the characteristic based total variation diminishing (TVD), artificial compressibility method (ACM) and Jameson methods. Results show that the ACM and TVD methods captured the shock waves with higher resolution than the Jameson method. Moreover, not only quality of shock wave capturing was improved for all flows at the discontinuities by employing ACM and TVD methods, but also the computational time and convergence were improved for the supersonic flows.

Keywords: Shock wave, Riemann solution, ACM, TVD, Jameson.

1 Introduction

The phenomenon of capturing of sharp gradients, shock waves, and contact discontinuities in compressible aerodynamic flows has been the subject of many researches and developments [1-24]. To cover this gap, various high-resolution schemes such as the total variation diminishing (TVD) technique [1] and Jameson's artificial dissipation method (ACM) [2] have been devised. Most of these schemes have been implemented in the density-based numerical algorithms. Numerical methods used in aerospace applications to carry out all computation processes associated with the compressible flows have reached to a very high level of maturity in terms of accuracy and efficiency. Currently, there are two main approaches dedicated to the development of algorithms that are valid for the flow computations at all velocities. The first one is the modification of compressible solvers (density-based) applicable for low Mach numbers. The second one is extension of the classical incompressible solvers (pressure-based) to the compressible flow. The main drawback of high-resolution schemes such as TVD method

[*]Corresponding Author, PhD, Department of Mechanical Engineering, K.N.Toosi University, Tehran, Iran, m.yadegari@kntu.ac.ir

[†]Assistant Professor, Department of Mechanical Engineering, Azarbaijan Shahid Madani University, Tabriz, Iran, jahdi@azaruniv.ac.ir

Receive : 2020/06/11 Accepted : 2021/04/12

is the smeary feature of discontinuities. The accuracy of these schemes across a sharp gradient is reduced to the first-order to prevent the non-physical oscillations and instabilities. Harten [3,4] introduced a method for calculation of discontinuous solutions of a single conservation law of hyperbolic systems by applying standard first-order schemes that dealt effectively with both shock and contact discontinuities. The method consists of two stages. In the first stage, the standard first-order scheme provides a monotonic variation of the solution near the sharp gradients. In the second stage, an artificial compression is applied to sharpen the transitions at discontinuities. Herten also formulated the ACM method based on primitive variables.

Yee et al. [5] extended the Harten's first-order ACM scheme to the TVD method by different context. So that, instead of switching from the second-order scheme to the first-order one for shock capturing, the order of accuracy remains acceptable and is capable of accurately capturing the steep gradients. Yee et al. [6] employed the ACM switch directly into the dissipation term of the TVD scheme and applied it to the computation of vortex convections as well as shock, shear and turbulence interactions. In their work, the flow was viscous and the discontinuities like shocks were computed by using direct numerical simulation (DNS) method. Also, they applied the entropy splitting method to discretize equations in order to overcome the instability issues. Therefore, the reduction of dissipation term does not induce any problem regarding the stability of the solution. Besides, Lie and Noelle [7] applied the ACM as a "limiter" to the high-order central difference scheme to improve the resolution of linear discontinuities. They used this method for computation of linear advection and unsteady one-dimensional gas dynamic equations and found these limiters as disadvantageous when they are applied to nonlinear fields. Yadegari and Abdollahi Jahdi [8] investigated the shock capturing by numerical dissipation on symmetric airfoil. They found that TVD method had a good quality in the shock wave capturing in comparison with the previously data obtained by density-based methods, while it had a less accuracy relative to the ACM. Recently, several authors have employed the TVD technique in the pressure-based algorithms. Lien and Leschziner [9] introduced a MUSCL (van Leer [10]) type of the TVD scheme into their developed pressure-based procedure. The slope limiter in their work relies on the gradients of the dependent variables. Shyy and Thakur [11] developed a scheme, what they called the controlled variation scheme (CVS), which was based on the formalism of the TVD concept applicable for the context of incompressible flow. The authors concluded that the existing TVD schemes are not generally applicable for the pressure-based methods for two reasons. First and foremost, unlike the simultaneous algorithms that treat gradients as part of the flux vectors, the TVD schemes are related to the contemporary sequential-iteration solution methods that treat the pressure–gradients as source terms in the momentum equations. Second, there are no definitions for local characteristics in which the flux limiters of the TVD schemes are based upon that. Thakur et al. [12] extended applications of their developed CVS scheme to the compressible flows including shocks as well as the incompressible flows. In the above-reviewed studies, the gradients of the either conserved or primitive variables are used in formulating the flux-limiting function. Indeed, Mulder and Van Leer [13] and Lin and Chieng [14], who carried out extensive numerical experiments, found the best accuracy by using the Riemann variables (at least for one-dimensional flows).

This might be because of the fact that only one of these variables can undergo a small change through a wave or a contact front, whereas large changes take place in the conserved or primitive variables. Issa and Javareshkian [15,16] were among the first to employ a high-resolution TVD scheme with characteristic variables-based flux limiters to a pressure-based finite volume method which solves Euler and Navier–stokes equations in the local coordinate system. The scheme was applied to transient one-dimensional and steady-state two-dimensional compressible flows. In addition to the study of Issa and Javareshkian [16], Kobayashi and Pereira [17] also introduced the characteristic-based flux computations into pressure-correction

solution procedures. They used the essentially non-oscillatory (ENO) scheme for the flux calculation and incorporated it into a steady state solution method.
Turkel et al. [18,19] and Guillard and Viozat [20] introduced the preconditioning techniques and identified that the discretized solution of the compressible fluid flow equations may fail to provide an accurate approximation for the incompressible flow equations at low Mach numbers. Also, more recently, Razavi and Zamzamian [21] presented an artificial compressible method to solve incompressible flow equations, using a density-based algorithm.
On the other hand, the main important part of the finite volume method is calculation of the conserved fluxes (i.e., mass, energy, momentum, etc.) in the cell walls. Researchers have introduced numerous methods to calculate these fluxes in more accurate and low-cost ways. For the first time, for instance, Godunove [22] used Riemann solution to compute theses conserved fluxes. The problem of Godunov method was direct use of the Riemann equation with its exact solution which remarkably increases the calculations time. Roe [23] used an approximate method based on the Godunov method to solve the Riemann equation, using a new interpolation approach for linearization (also called Roe interpolation method). Colella and Woodward [24] considered the idea of using both first order flux and anti-diffusion terms as limiting fluxes. In this procedure, the calculated optimal anti-diffusion is added to the first order flux. In this paper, we will analyze the influence of the ACM on the flow computation from the view point of accuracy, computational cost and convergency of the solution in supersonic flows over bump with Mach numbers of 1.4, 1.65. Finally, we will show that the ACM not only improves the resolution of shocks in all cases, but also accelerates the convergency of solutions in supersonic flows.

2 Governing equations and finite volume discretization

In this section, the mathematical formulations of governing equations for an inviscid compressible flow are discussed. For a flow passing through a volume Ω limited to an area Γ, the Euler equations are written as follows:

$$\frac{\partial}{\partial t}\int_{\Omega}\rho\, d\Omega+\oint\rho\vec{v}\, d\vec{\Gamma}=0 \tag{1}$$

$$\frac{\partial}{\partial t}\int_{\Omega}\rho\vec{v}\, d\Omega+\oint(\rho\vec{v}\otimes\vec{v}+P)\, d\vec{\Gamma}=\int_{\Omega}\rho\vec{f}_e\, d\Omega \tag{2}$$

$$\frac{\partial}{\partial t}\int_{\Omega}\rho E\, d\Omega+\oint\rho H\vec{v}\cdot d\vec{\Gamma}=\int_{\Omega}\rho\vec{f}_e\cdot\vec{v}\, d\Omega \tag{3}$$

In Eqs. (1-3), ρ is density, $\vec{v}$ is the velocity vector, P is pressure, $\vec{f}_e$ represents all external forces, E is internal energy, and H is the total enthalpy of the fluid that can be expressed in terms of Eq.(4):

$$h=c_pT\ ,\ H=h+\frac{|\vec{v}|^2}{2} \tag{4}$$

The total internal energy E is defined as $E=e+\frac{|\vec{v}|^2}{2}$, where e is $e=c_vT$ and c_v is the specific heat at constant volume. All above equations can be defined in a general matrix form. Hereby, by considering U as the conservative variable tensor, $\vec{F}$ as the flux vector, and $\bar{I}$ as the unit matrix, it can be written follows:

$$U=\begin{bmatrix}\rho\\ \rho\vec{v}\\ \rho E\end{bmatrix}\ ,\ F=\begin{bmatrix}\rho\vec{v}\\ \rho\vec{v}\otimes\vec{v}+P\bar{I}\\ \rho\vec{v}H\end{bmatrix},Q=\begin{bmatrix}0\\ \rho\vec{f}_e\\ \rho\vec{f}_e\cdot\vec{v}\end{bmatrix} \tag{5}$$

$$\frac{\partial}{\partial t}\int_{\Omega}U\,d\Omega+\oint\vec{F}\,d\vec{\Gamma}=\int_{\Omega}Q\,d\Omega$$

By re-writing Eq. (5) in the differential form, we have:

$$\frac{\partial U}{\partial t}+\vec{\nabla}\cdot\vec{F}=Q \tag{6}$$

For a 2D steady flow, the Cartesian components of U and F vector are described by Eq.(7):

$$U=\begin{bmatrix}\rho\\ \rho u\\ \rho v\\ \rho E\end{bmatrix},\ f=\begin{bmatrix}\rho u\\ \rho u^2+P\\ \rho uv\\ \rho uH\end{bmatrix},\ g=\begin{bmatrix}\rho v\\ \rho uv\\ \rho v^2+P\\ \rho vH\end{bmatrix} \tag{7}$$

Where, u and v are the velocity components of $\vec{v}$ in x and y directions, respectively. Thus, Eq. (6) can be written in the Cartesian coordinate form as follows:

$$\frac{\partial U}{\partial t}+\frac{\partial f}{\partial x}+\frac{\partial g}{\partial y}=Q \tag{8}$$

Equation (8) is known as the Euler equation.

3 Calculation of flux in an oblique surface

The computational cells are not always diagonal and the cells' lines are not in direction of the flow, especially in applied problems. Therefore, the flux flowing through the surface of the cell can have both x and y components. Thus, the equations and calculation procedure of the fluxes should be changed. In the most previous works conducted by Harten [1,3-4], Yee [5-6], the matrices of the left and right agent vectors and other flux parameters were separately used in x and y directions. After all calculations, the parameters were converted from local coordinate to the main one. Since the cells and governing equations are discretized based on the finite volume method and the computational cell is the same as the physical cell, the Hirch method is used to calculate these fluxes. Through this calculation process, all flux terms and their elements in the location directions of $\zeta=\zeta(x,y)$ and $\eta=\eta(x,y)$ are decomposed to x and y directions, and then are summed together. Thus, it is necessary to investigate the effects of the cell geometry and its surface position relative to the center of the surrounding cells. The geometry used in calculating the flux is shown in Figure (1).

3-1 Calculation of flux at e surface

In order to calculate the passing flux in the e surface of the cell, the surface shown in Figure (1) is considered. When this surface is individually investigated, an arbitrary position of the surface in the locational coordinate (ζ,η) is related to the main coordinate (x,y), as shown in Figure (2).

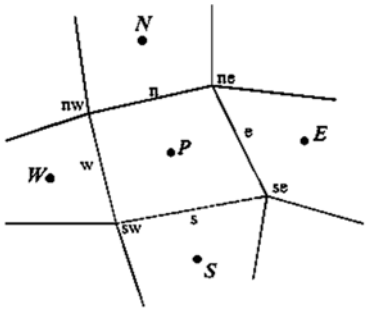

Figure 1 Geometry used in calculating the flux

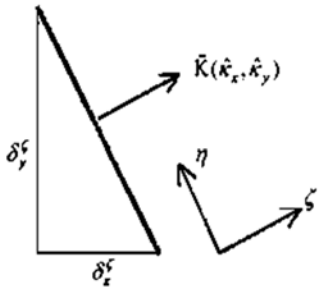

Figure 2 Cell surface e in the local coordinates

The geometrical equations defined in Figure (2) can be written as follows:

$$\vec{\mathrm{K}} = \frac{\vec{\nabla}\zeta}{\left|\vec{\nabla}\zeta\right|} = \hat{\kappa}_x \vec{i} + \hat{\kappa}_y \vec{j}$$
$$l = \sqrt{(\delta_x^\zeta)^2 + (\delta_y^\zeta)^2} \tag{9}$$
$$\hat{\kappa}_x = \delta_x^\zeta / l$$
$$\hat{\kappa}_y = \delta_y^\zeta / l$$

In Eq. (9), $\hat{k}_{\mathrm{x}}$ and $\hat{k}_y$ are the Cartesian components of unit vector of $\vec{k}$. This unit vector is perpendicular to the surface of the cell, and is in direction of the local coordinate. According to the symbols of Figure (1), δ_y^ζ ,δ_x^ζ can be written respectively as :

$$\delta_x^\zeta = y_{ne} - y_{se} \tag{10}$$
$$\delta_y^\zeta = -(x_{ne} - x_{se})$$

Flux of the velocity vector in ζ direction can be defined in terms of Eq. (11).

$$V^\zeta = u\delta_x^\zeta + v\delta_y^\zeta \tag{11}$$

The conservative vector of variables and the conservative vector of mass flux, momentum, and energy in the center of each surrounding cell of the e surface are indicated by U and F^ζ respectively as follows:

$$U = (\rho\ ,\ \rho u\ ,\ \rho v\ ,\ \rho E)^T$$
$$F^{\zeta} = \begin{bmatrix} \rho V^{\zeta} \\ \rho V^{\zeta} u + P\delta_x^{\zeta} \\ \rho V^{\zeta} v + P\delta_y^{\zeta} \\ \rho V^{\zeta} H \end{bmatrix} \tag{12}$$

For an arbitrary cell, flux at the e surface is determined by Eq. (13).

$$F_e = \frac{1}{2}(F_L^{\zeta} + F_R^{\zeta}) - \frac{1}{2}\sum_{i=1}^{4} r_i \left|\lambda_i\right| \alpha_i \tag{13}$$

where, λ_i is the agents value and α_i refers to the characteristic variables. In the hyperbolic equations system, the four agents at the appointed surface for a 2D flow are:

$$\begin{cases} \lambda_1 = \widetilde{V}^{\zeta} \times l \\ \lambda_2 = \widetilde{V}^{\zeta} \times l \\ \lambda_3 = (\widetilde{V}^{\zeta} + \widetilde{c}) \times l \\ \lambda_4 = (\widetilde{V}^{\zeta} - \widetilde{c}) \times l \\ \widetilde{V}^{\zeta} = \widetilde{u}\,\hat{\kappa}_x + \widetilde{v}\,\hat{\kappa}_y \end{cases} \tag{14}$$

The characteristic values of α at the e surface are computed by multiplying each row of the left agent matrix $\tilde{P}^{-1}$ by the conservative variables ΔU :

$$\begin{cases} \Delta U = ((\rho_R - \rho_L),(\rho_R u_R - \rho_L u_L),(\rho_R v_R - \rho_L v_L),(\rho_R E_R - \rho_L E_L))^T \\ \alpha_1 = \widetilde{P}_e^{-1}(1,:)\,\Delta U \\ \alpha_2 = \widetilde{P}_e^{-1}(2,:)\,\Delta U \\ \alpha_3 = \widetilde{P}_e^{-1}(3,:)\,\Delta U \\ \alpha_4 = \widetilde{P}_e^{-1}(4,:)\,\Delta U \end{cases} \tag{15}$$

Eq. (15) is written in general form and its vector form can be defined by Eq. (16).

$$\alpha_e = \widetilde{P}_e^{-1}(U_E - U_P) \tag{16}$$

Also, in Eq. (15), the subscripts *L* and *R* are used to indicate the center of left and right cells of the e surface, respectively. $\widetilde{P}_e^{-1}(i,:)$ is the ith row of the left agent matrix $\widetilde{P}^{-1}$ and the sign ~ indicates that the matrix is defined at the surface of the e cell and its components are based on the Roe averaging method, as defined in Eq. (17). Moreover, r_i in Eq. (13) is the ith column of $\tilde{P}$ (also expressed in Eq. (17)).

$$\tilde{P}=\begin{bmatrix} 1 & 0 & \frac{\tilde{\rho}}{2\tilde{c}} & \frac{\tilde{\rho}}{2\tilde{c}} \\ \tilde{u} & \tilde{\rho}\hat{\kappa}_y & \frac{\tilde{\rho}}{2\tilde{c}}(\tilde{u}+\tilde{c}\hat{\kappa}_x) & \frac{\tilde{\rho}}{2\tilde{c}}(\tilde{u}-\tilde{c}\hat{\kappa}_x) \\ \tilde{v} & -\tilde{\rho}\hat{\kappa}_x & \frac{\tilde{\rho}}{2\tilde{c}}(\tilde{v}+\tilde{c}\hat{\kappa}_y) & \frac{\tilde{\rho}}{2\tilde{c}}(\tilde{v}-\tilde{c}\hat{\kappa}_y) \\ \frac{\tilde{\vec{V}}^2}{2} & \tilde{\rho}(\tilde{u}\hat{\kappa}_y-\tilde{v}\hat{\kappa}_x) & \frac{\tilde{\rho}}{2\tilde{c}}(\tilde{H}+\tilde{c}\tilde{\vec{V}}\cdot\vec{\mathrm{K}}) & \frac{\tilde{\rho}}{2\tilde{c}}(\tilde{H}-\tilde{c}\tilde{\vec{V}}\cdot\vec{\mathrm{K}}) \end{bmatrix} \tag{17}$$

$$\tilde{P}^{-1}=\begin{bmatrix} 1-\frac{\gamma-1}{2}\tilde{M}^2 & (\gamma-1)\frac{\tilde{u}}{\tilde{c}^2} & (\gamma-1)\frac{\tilde{v}}{\tilde{c}^2} & -\frac{\gamma-1}{\tilde{c}^2} \\ \frac{1}{\tilde{\rho}}(\tilde{v}\hat{\kappa}_x-\tilde{u}\hat{\kappa}_y) & \frac{\hat{\kappa}_y}{\tilde{\rho}} & \frac{-\hat{\kappa}_x}{\tilde{\rho}} & 0 \\ \frac{\tilde{c}}{\tilde{\rho}}(\frac{\gamma-1}{2}\tilde{M}^2-\frac{\tilde{\vec{V}}\cdot\hat{\kappa}}{\tilde{c}}) & \frac{1}{\tilde{\rho}}[\hat{\kappa}_x-(\gamma-1)\frac{\tilde{u}}{\tilde{c}}] & \frac{1}{\tilde{\rho}}[\hat{\kappa}_y-(\gamma-1)\frac{\tilde{v}}{\tilde{c}}] & \frac{\gamma-1}{\tilde{\rho}\tilde{c}} \\ \frac{\tilde{c}}{\tilde{\rho}}(\frac{\gamma-1}{2}\tilde{M}^2+\frac{\tilde{\vec{V}}\cdot\hat{\kappa}}{\tilde{c}}) & -\frac{1}{\tilde{\rho}}[\hat{\kappa}_x+(\gamma-1)\frac{\tilde{u}}{\tilde{c}}] & -\frac{1}{\tilde{\rho}}[\hat{\kappa}_y+(\gamma-1)\frac{\tilde{v}}{\tilde{c}}] & \frac{\gamma-1}{\tilde{\rho}\tilde{c}} \end{bmatrix}$$

Based on the second order upwind TVD approximation, Yee et al. [5, 6] proposed Eq. (18) for spatial displacement discretization of the diffusion term.

$$\phi_e^l=\frac{1}{2}\psi(\lambda_e^l)(g_E^l+g_P^l)-\psi(\lambda_e^l+\gamma_e^l)\alpha_e^l \tag{18}$$

where, the γ function is defined by Eq. (19):

$$\gamma_e^l=\frac{1}{2}\psi(\lambda_e^l)\begin{cases}\frac{g_E^l-g_P^l}{\alpha_e^l}, & \alpha_e^l\neq 0\\ 0, & \alpha_e^l=0\end{cases} \tag{19}$$

In Eq. (19), λ_e^l is the value of the l[th] characteristic at the e surface of the cell, g_i^l is the limited function related to the l[th] characteristic at the center of the i[th] cell, α_e^l is the characteristic variable at the e surface of the cell which is equal to the l[th] column of $\tilde{P}^{-1}\Delta U$, and ψ is the enthalpy function. Harten [1] suggested the above assumption in terms of .Eq. (20).

$$\psi(a_e^l)=\begin{cases}\left|a_e^l\right| & \left|a_e^l\right|\geq\varepsilon_1\\ \left[(a_e^l)^2+\varepsilon_1^2\right]/2\varepsilon_1 & \left|a_e^l\right|<\varepsilon_1\end{cases} \tag{20}$$

In Eq. (20), ε_1 is zero for flow containing dynamic shock waves and is negligible for static shock waves. Various functions have been considered for the limited function g_i^l at the cell center. For instance, Yee et al. [6] suggested the following expression for that:

$$g_P^l = \text{minmod}(\alpha_e^l, \alpha_w^l)$$
$$where\ \text{minmod}(x,y) = sign(x)\cdot\max\left\{0, \min\left[|\ x\ |, y\cdot sign(x)\right]\right\} \tag{21}$$

In order to avoid any problem during the computations, Yee et al. [6] introduced Eq. (22) for the enthalpy and gamma functions ($\varepsilon = 10^{-7}, \delta = 0.0625$).

$$\psi(z) = \sqrt{\left(\delta + z^2\right)}$$
$$\gamma_{i+1/2}^l = \frac{1}{2}\frac{\psi(a_{i+1/2}^l)(g_{i+1}^l - g_i^l)\alpha_{i+1/2}^l}{(\alpha_{i+1/2}^l)^2 + \varepsilon} \tag{22}$$

4 Reduction of TVD error using ACM

As it is explained, when discontinuities occur, high resolution methods such as TVD and ENO prevent from creation of the oscillations by means of order of reduction which itself increases the diffusion. Hereby, the accuracy of the shock waves capturing scheme is decreased in the discontinuities. Therefore, finding a method for modifying this phenomenon is essential. Harten [3-4] introduced a new method to increase the accuracy of the first order scheme in the shock wave capturing around the discontinuities zones. Yee et al. [6] used this method for viscous flow as :

$$F_{i+1/2} = \frac{1}{2}[F_{i+1} + F_i + R_{i+1/2}\Phi^*_{i+1/2}] \tag{23}$$

In Eq. (23), the diffusion function is combined by the TVD and anti-diffusion functions (Harten switch) [3-4] in which the anti-diffusion function is directly imposed on it, as expressed below:

$$\phi^{l*}_{i+1/2} = \kappa\theta^l_{i+1/2}\phi^l_{i+1/2} \tag{24}$$

$$\theta_i^l = \frac{\left|\left|\alpha_{i+1/2}^l\right| - \left|\alpha_{i-1/2}^l\right|\right|}{\left|\alpha_{i+1/2}^l\right| + \left|\alpha_{i-1/2}^l\right| + \varepsilon} \tag{25}$$

where, ϕ_i^l is the anti-diffusion function at the surface of the ith cell and is related to the lth characteristic and k is a coefficient that highly depends on the physics of the problem. In this study, in order to increase the accuracy and decrement of diffusion in discontinuities, another approach is considered in terms of imposing the ACM to the diffusion term of TVD. By noticing to the previous points, we can state that ACM cannot be imposed directly on diffusion term. Therefore, the anti-diffusion function is imposed on the diffusion term of the limited function, which affects it accordingly. The utilized method can be expressed in terms of Eq. (26):

$$\tilde{g}_i^l = (1+\omega^l\theta_i^l)g_i^l \quad ,\ \omega > 0 \tag{26}$$

As can be seen, the g function is replaced by the generated limited function in the diffusion term of TVD. Also, in Eq. (26), ω is the coefficient of ACM. Because each wave (linear and nonlinear waves) has a specific diffusion, we have different coefficients for each characteristic relative to each other. θ_i^l for each characteristic of *l* in the ith cell is defined as follows:

$$\theta_i^l = \frac{\left|\alpha_{i+1/2}^l - \alpha_{i-1/2}^l\right|}{\left|\alpha_{i+1/2}^l\right| + \left|\alpha_{i-1/2}^l\right| + \varepsilon} \tag{27}$$

where, α is the characteristic variable computed at the surface of the cell and ω is a coefficient that is different for various characteristics and is function of flow's physics. Thus, it is calculated by trial-and-error method for specific flow. Based on the reviewed equations, it can be claimed that the new limited function ($\hat{g}$) is greater than the limited function of TVD method. As a result, the accuracy and convergence of solution are improved, thereby improving the shock wave capturing phenomenon. But, with increment of ω and consequently the limited function, the diffusion is decreased too and the convergence procedure can probably be interrupted. Thus, ω should be defined in a specific range or should have an optimum value for specific flow, in which in that values the increment of the accuracy doesn't occur along with more convergence reduction and computation time increment, which is discussed in the next section.

5 Problem statement

The present study analyze a 2D steady state flow over a circular bump under a supersonic flow with M=1.4 and 1.65 (suitable for compressible flows). The thickness of the circular arc "bump" on the upper wall is 4% of the bump length. The geometry of a 4% thick bump on a channel wall along with the algebraic mesh (90×30) are shown in Figure (3). The length of the computational meshing is assumed 3m with 30 nodes in the y-direction and 90 nodes in the x-direction. The bump is located in the northern boundary.

6 Solution independency from grid size

The effect of grid nodes number on pressure distribution and Mach number is shown in Tables (1-2). As it is seen, the variations of pressure and Mach number with grid nodes number of 90× 30 become independent from grid size.

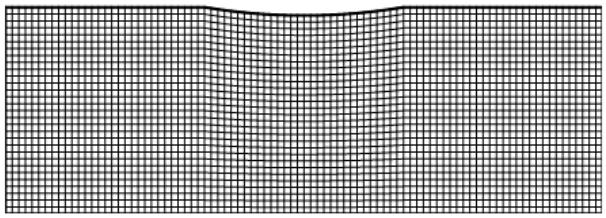

Figure 3 Supersonic flow over 4% thick bump ($M_{in} = 1.4$ and 90×30 mesh)

Table 1 The effect of grid nodes number on pressure distribution.

Case	grid nodes	Jameson method	TVD method	ACM method
Supersonic, M = 1.4	80× 20	142251.394	144155.05	141968.3943
	90× 30	147163.125	137469.12	136320.2058
	120× 40	147408.261	137382.23	136624.2014
	140× 60	147653.397	137296.34	136928.1969

Table 2 The effect of grid nodes number on Mach number distribution.

Case	grid nodes	Jameson method	TVD method	ACM method
Supersonic, M = 1.4	80× 20	1.4020	1.3903	1.4010
	90× 30	1.3817	1.4184	1.4264
	120× 40	1.3813	1.41805	1.42325
	140× 60	1.381	1.4177	1.4201

7 Numerical Method

The finite volume method is applied to discretize the governing equations and considering the compressible flow, the base density method is used. The flow is assumed two dimensional steady state and explicit segregated algorithm approach is employed to solve the equations.
A multi-stage, time-stepping algorithm is used to discretize the time derivative. The solution is advanced from iteration to iteration with an stage Rung-Kutta scheme, given by:

$$w_i^{(0)} = w_i^{(n)} \tag{28}$$

$$w_i^{(1)} = w_i^{(0)} - \frac{\alpha_1 \Delta t_i}{A_i} R_i'\left(w_i^{(0)}\right) \tag{29}$$

$$w_i^{(2)} = w_i^{(0)} - \frac{\alpha_2 \Delta t_i}{A_i} R_i'\left(w_i^{(1)}\right) \tag{30}$$

$$w_i^{(3)} = w_i^{(0)} - \frac{\alpha_3 \Delta t_i}{A_i} R_i'\left(w_i^{(2)}\right) \tag{31}$$

$$w_i^{(4)} = w_i^{(0)} - \frac{\alpha_4 \Delta t_i}{A_i} R_i'\left(w_i^{(3)}\right) \tag{32}$$

$$w_i^{(n+1)} = w_i^{(4)} \tag{33}$$

In addition, the convergence criterion for equations of continuity and momentum, is considered equal to 10^{-6}.

8 Results and discussion

This section discusses on the results obtained from numerical analysis of inviscid flow solved by Jameson, TVD, and ACM methods and compares them all with each other. The effect of numerical diffusion reduction on the results is also explained.

8-1 Supersonic flow with Mach 1.4

In this section, the results of simulation for a supersonic, steady state, and inviscid flow over a bump with the thickness of 4% are presented. Figures (4-5) illustrate the distribution of the Mach number through the upper and lower walls for each three method, respectively. Figures (6-7) indicate the pressure distribution through the upper and lower walls for each three method, respectively.
According to Figures (4-7), the decrement rate of diffusion has increased the numerical accuracy in computation of the Mach number and pressure in locations where the reflection of waves occur. The contours of the Mach number are indicated in Figures (8-10) in order to show the increment of the solution accuracy in the whole computation domain.

As it observed, all waves captured by the ACM, including shock waves propagation, waves interaction, and waves reflection from walls are better than those captured by the TVD and Jameson methods, underlining the innovation and accuracy of the applied method.

A comprehensive comparison upon the above figures illustrates the effectiveness of ACM and its high efficiency at the discontinuities. For TVD and Jameson methods, the Mach number contours are dispersed at the shock wave location due to the high values of numerical diffusion. On the other hand, dispersion effects in the ACM method are decreased and the shock wave is captured more accurately since the numerical diffusion is decreased.

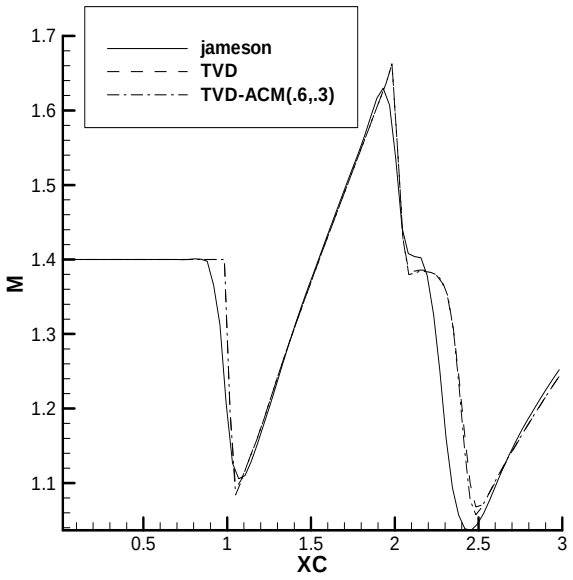

Figure 4 Mach number profile through the upper wall

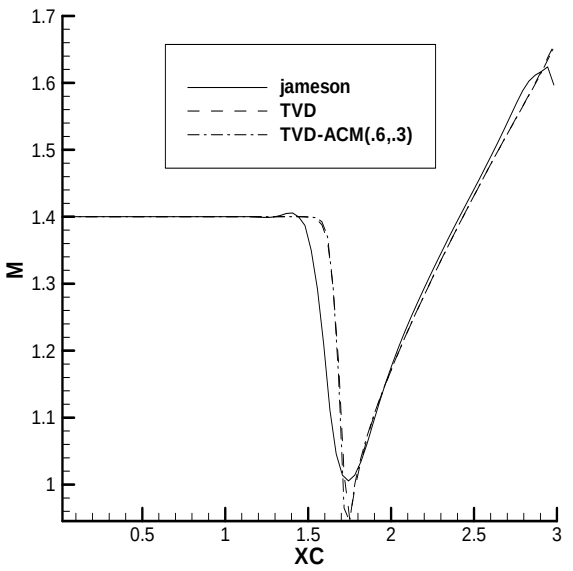

Figure 5 Mach number profile through the lower wall

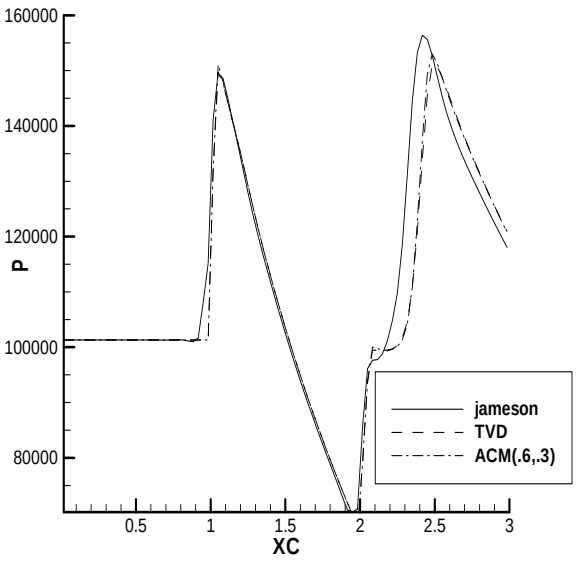

Figure 6 Pressure distribution through the upper wall

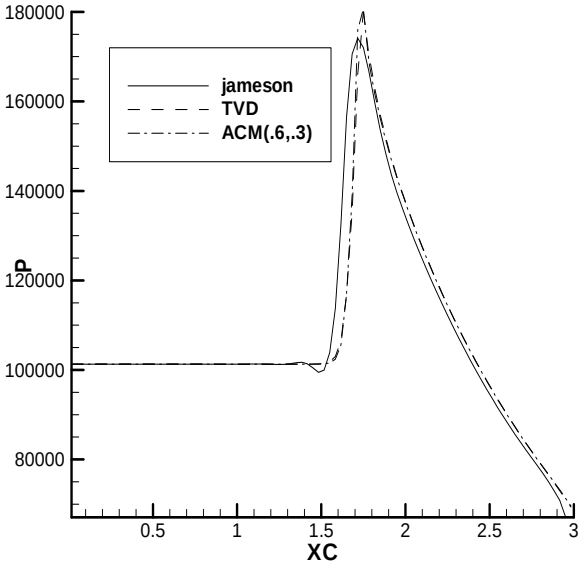

Figure7 Pressure distribution through the lower wall

It is noteworthy to pinpoint that all physical and computational conditions for all three methods are the same, and the way of imposing the coefficients and anti-diffusion function on the limited function in the ACM are only different.
The pressure contours for each three method are displayed in Figures (11-13).

8-2 Supersonic flow with Mach 1.65

Figures (14-15) show the distribution of the Mach number through the upper and lower walls for M=1.65. The pressure distribution on the upper and lower boundaries of the channel is displayed in Figures (14-15), respectively. Figures (18-20) show the contour of the Mach number inside the channel, and Figures (21-23) show the pressure contour for all three methods.

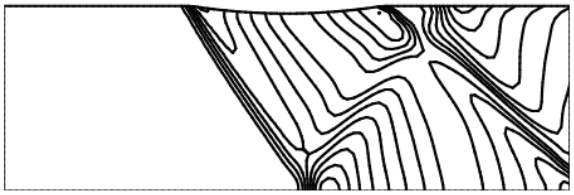

Figure8 Mach number contours (Jameson)

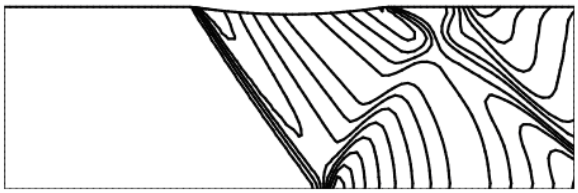

Figure 9 Mach number contours (TVD)

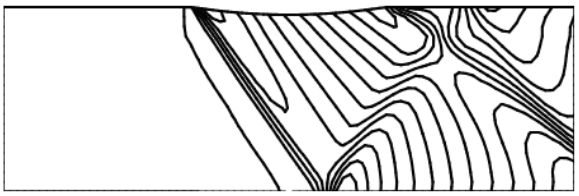

Figure 10 Mach number contours (TVD-ACM)

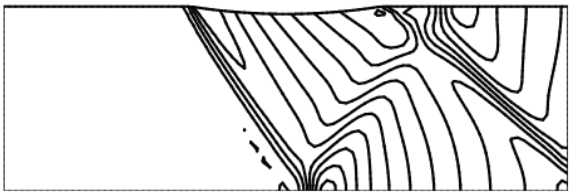

Figure 11 Pressure contours (Jameson)

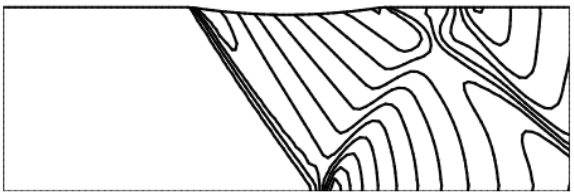

Figure 12 Pressure contours (TVD)

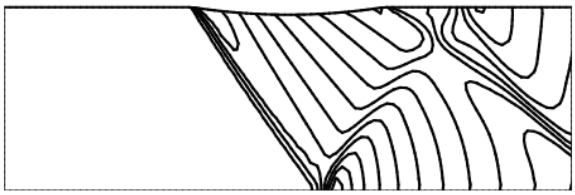

Figure 13 Pressure contours (TVD-ACM)

Although the density-based algorithm is suitable for compressible flows, Figure (18) does not show a convenient capturing of the shock wave. Refraction is observed at the outlet due to the poor boundary condition or its lower order, while all waves including propagation of shock waves, interaction between waves, and reflection from walls are better captured at the outlet by TVD and ACM methods.

It is also observed that capturing the reflected shock wave from the upper wall and the outlet waves is improved by imposing the anti-diffusion function on the ACM.

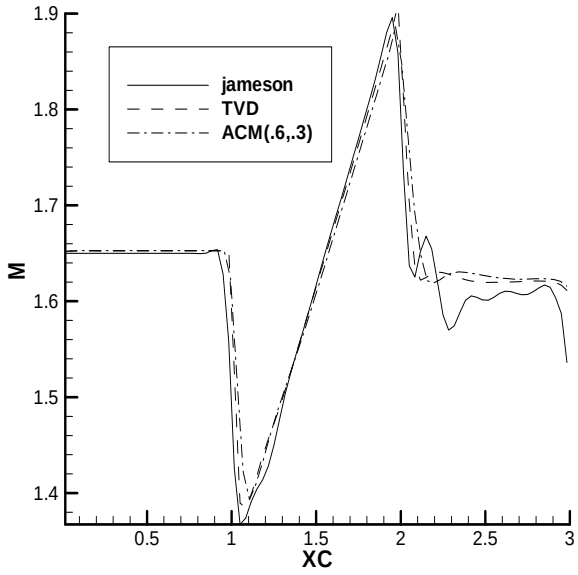

Figure 14 Mach number profile through the upper wall

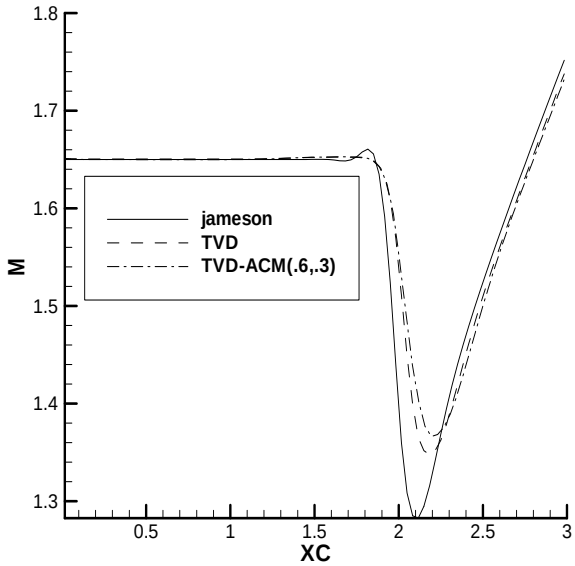

Figure 15 Mach number profile through the lower wall

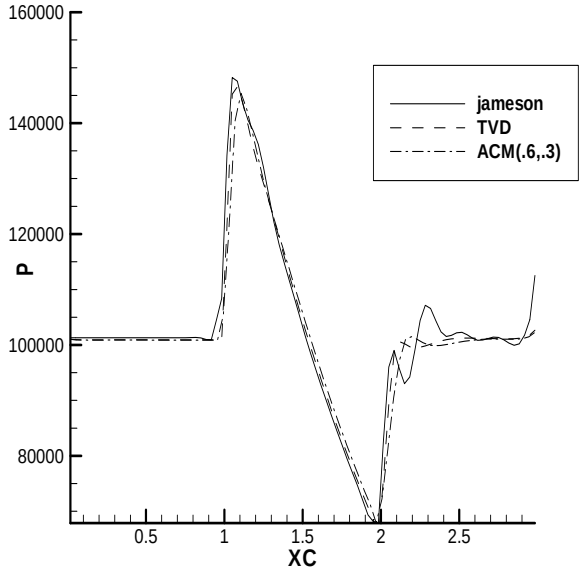

Figure 16 Pressure distribution through the upper wall

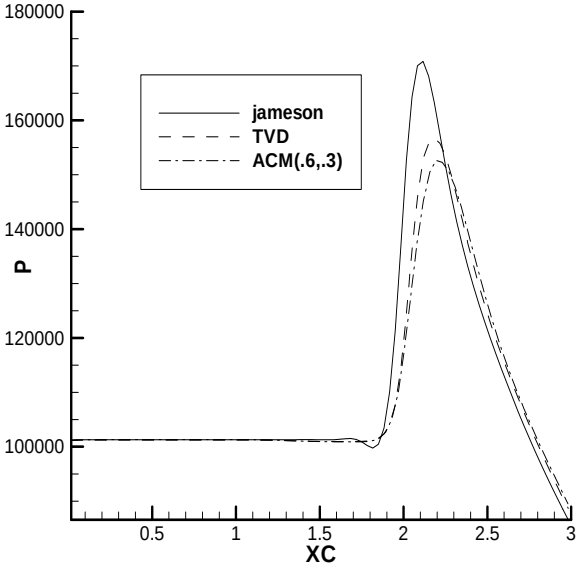

Figure 17 Pressure distribution through the lower wall

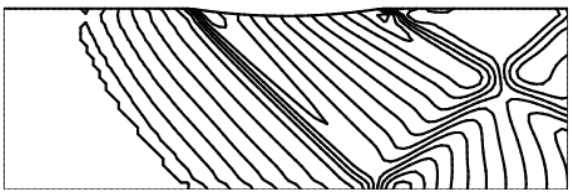

Figure 18 Mach *number contours (Jameson)*

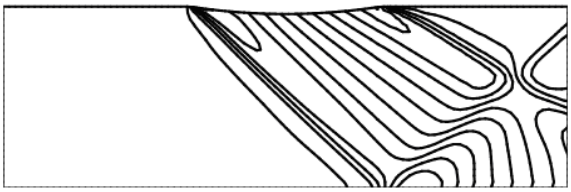

Figure 19 Mach number contours (TVD)

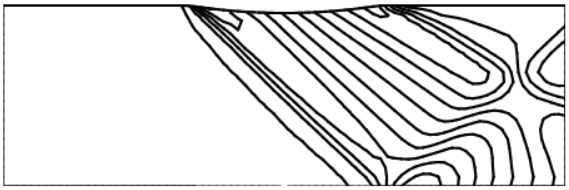

Figure 20 Mach number contours (TVD-ACM)

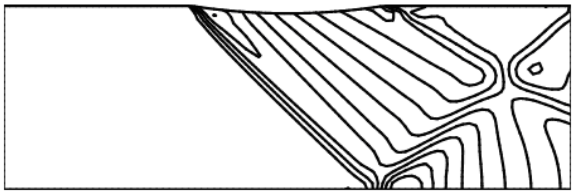

Figure 21 Pressure contours (Jameson)

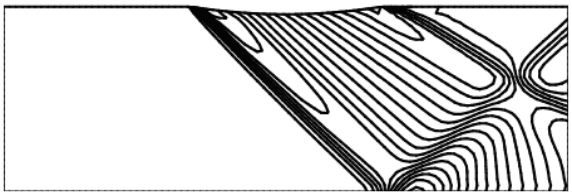

Figure 22 Pressure contours (TVD)

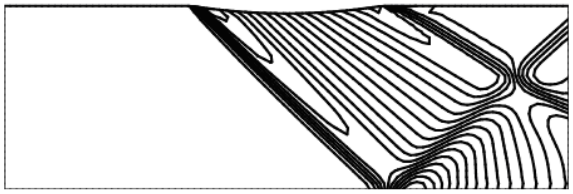

Figure 23 Pressure contours (TVD-ACM)

9 Comparing of solution convergence and computations time for TVD, Jameson, and ACM methods

This section investigates solution convergence and computational time related to the numerical solution of supersonic flow over the bump for each specific flow. Boundary condition and cell size are the same for each method, and the only difference is the way of imposing of the anti-diffusion function with various coefficients on the ACM method. The residual history of velocity for the supersonic case is shown in Figure (24). As can be observed in Figure (24), the solution convergence is achieved by more iterations for a specific accuracy relative to the TVD method since more operations and reduction in the numerical diffusion is observed by the ACM method in this flow. Note that, the first and second values in the parenthesis for the ACM are related to the anti-diffusion function for linear and nonlinear flow fields, respectively.
Figure (25) shows the convergence diagram at the supersonic flow with inlet Mach number of 1.4. By noticing to this diagram, it can be stated that the convergence of TVD method remains at the constant level after a specific iteration and becomes horizontal.
However, when the anti-diffusion function is imposed on the ACM, the convergence becomes better, and solution procedure is converged in lower accuracy. The effect of ACM coefficients is also important in solution convergence which is shown in Figure (26).
Thereby, by considering ω=0.27 for linear and ω=0.5 for nonlinear fields, the convergence rate can be improved. As a result, the quality of shock wave capturing is increased and diffusion in capture of discontinuities is decreased with the increment of ACM coefficients. But, it's difficult to conclude that the convergence is improved, because a large decrement in the numerical diffusion has a remarkable negative effect on the solution convergence. Thus, it's necessary to find optimum coefficients of the anti-diffusion function for each flow. Residual history of the velocity "u" for M=1.65 is shown in Figure (27).
As it was observed in Figure (27), an acceptable convergence is achieved within less iteration for lower residual target by imposing the anti-diffusion function on the computational processes of the ACM coefficients. Figure (28) shows the convergence diagram for M=1.65 at inlet of the bump channel. According to Figure (28), a significant convergence improvement is achieved for this flow for ACM coefficients of 0.9 and 0.5. Also, the number of iteration is reduced by around one per fifth for a specific residual target relative to the TVD method.

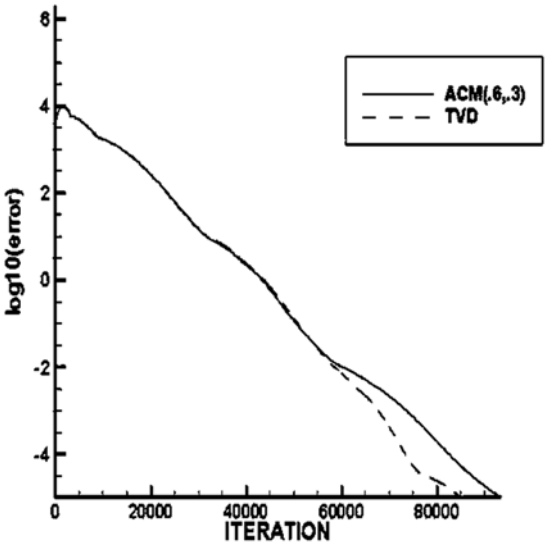

Figure 24 Residual history of velocity "u" for supersonic case .The numbers in parenthesis (0.6,0.3)correspond to ($\omega_{1,2}$,$\omega_{3,4}$) for ACM. (ω_1&ω_2) and (ω_3&ω_4) are considered for linear and nonlinear scopes, respectively.

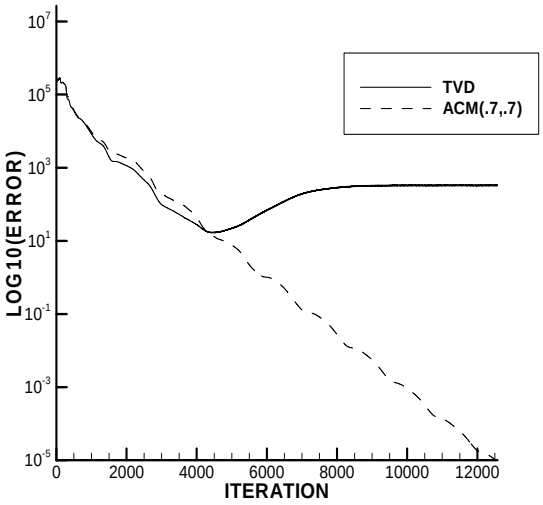

Figure 25 Residual history of velocity "u" for M=1.4. The numbers in parenthesis (0.7,0.7) correspond to ($\omega_{1,2}$,$\omega_{3,4}$) for ACM. (ω_1&ω_2) and (ω_3&ω_4) are considered for linear and nonlinear scopes, respectively

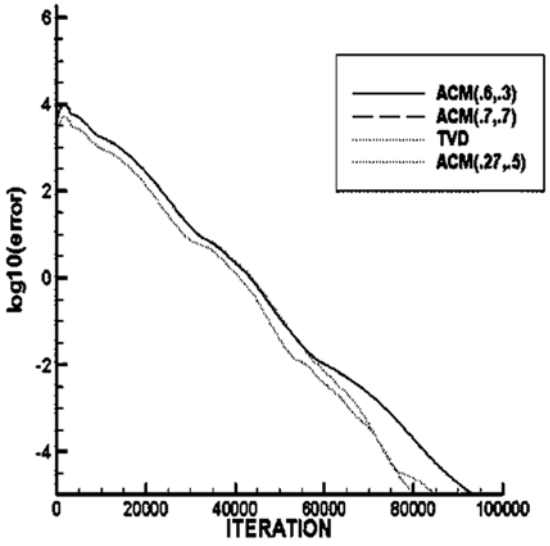

Figure 26 Residual history of velocity "u" for M=1.4. The numbers in parenthesis (0.7,0.7) and 0.27,0.5) and (0.6,0.3) correspond to ($\omega_{1,2}$,$\omega_{3,4}$) for ACM. (ω_1&ω_2) and (ω_3&ω_4) are considered for linear and nonlinear scopes, respectively

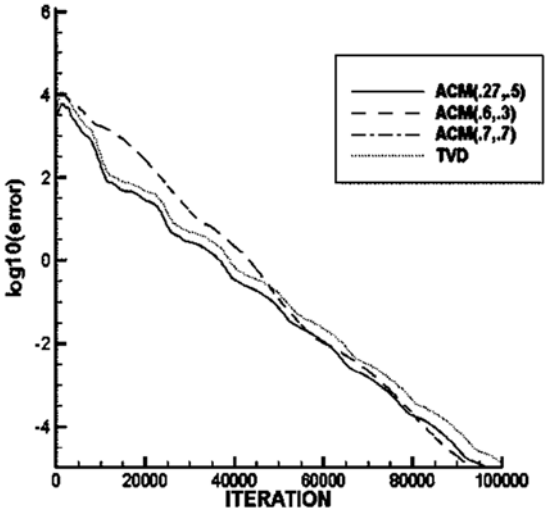

Figure 27 Residual history of velocity "u" for M=1.65. The numbers in parenthesis (0.7,0.7) and 0.27,0.5) and (0.6,0.3) correspond to ($\omega_{1,2}$,$\omega_{3,4}$) for ACM. (ω_1&ω_2) and (ω_3&ω_4) are considered for linear and nonlinear scopes, respectively

In order to investigate the effect of number of grids on the optimum coefficients of ACM, the supersonic flow with M=1.65 in the bump channel is chosen. The convergence diagram is shown in Figure (29), where all conditions except the grids are fixed for each case.

As Figure (29) indicates, it is obvious that the solution is not converged within an acceptable accuracy for the coarse grid. On the other hand, the solution convergence is improved by decrement of the ACM coefficients for nonlinear fields.

In this study, it is necessary to investigate the computational time for a specific accuracy or iteration. The results of this investigation are tabulated in Table (3), in which the computational time for various ACM coefficients are compared with those obtained by the TVD method. Tables (3-4) listed the CPU times for the supersonic flow over the bump channel. Accordingly, the convergence time of the ACM method for a specific iteration numbers of high enough which is mainly due to high number of operations and low numerical diffusion. It should be noted that this factor should not be considered for achieving the specified accuracy. According to Tables (3-4), the running time at the equivalent iteration is increased by 5% for the ACM method.
On the other hand, it cannot be concluded that for an arbitrary accuracy (see Figure (27)), the convergence rate achieved by the ACM method is faster than that obtained by the TVD method. Also, in order to avoid instability in solution convergence, the optimum values of anti-diffusion coefficients of nonlinear fields should be less than those of the linear fields.

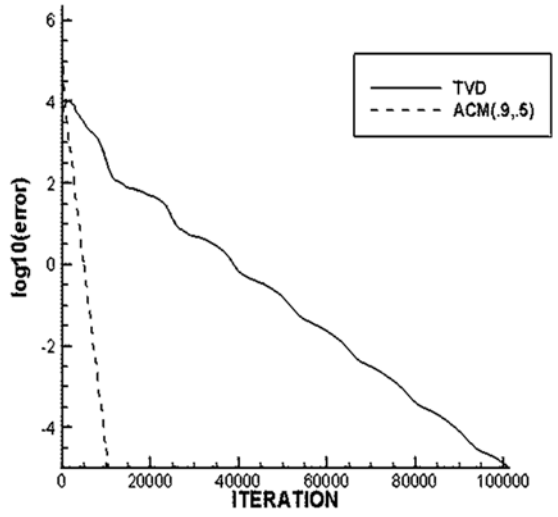

Figure 28 Residual history of velocity "u" for M=1.65. The numbers in parenthesis (0.9, 0.5) correspond to $(\omega_{1,2},\omega_{3,4})$ for ACM. $(\omega_1 \& \omega_2)$ and $(\omega_3 \& \omega_4)$ are considered for linear and nonlinear scopes, respectively

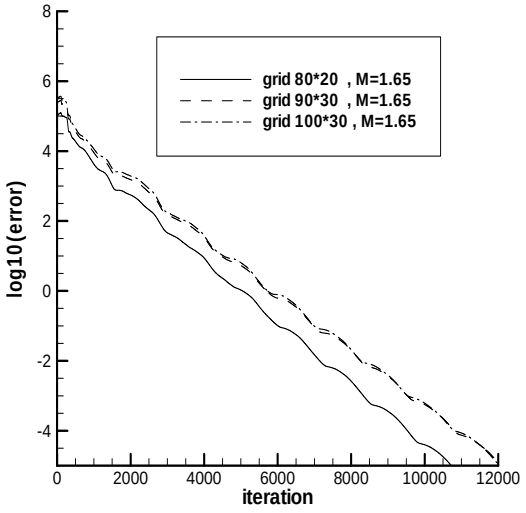

Figure 29 Residual history of velocity "u" for M=1.65 for different numbers of grid points

Table 3 CPU time (s) for supersonic case until 3,000 iterations.

Case	TVD Method	ACM method	ACM method	ACM method	ACM method	ACM method
		$\omega_{1,2}$=0.6 $\omega_{3,4}$=0.5	$\omega_{1,2}$ =0.6 $\omega_{3,4}$ =0.6	$\omega_{1,2}$=0.7 $\omega_{3,4}$=0.7	$\omega_{1,2}$=1.5 $\omega_{3,4}$=0.8	$\omega_{1,2}$=1.5 $\omega_{3,4}$=1.0
Supersonic, M = 1.4	409s	426s	427s	421s	421s	426s

Table 4 CPU time (s) for supersonic case until 3,000 iterations.

Case	TVD Method	ACM method	ACM method	ACM method	ACM method	ACM method
		$\omega_{1,2}$ =0.7 $\omega_{3,4}$=0.2	$\omega_{1,2}$=0.7 $\omega_{3,4}$=0.6	$\omega_{1,2}$=0.8 $\omega_{3,4}$=0.7	$\omega_{1,2}$=0.9 $\omega_{3,4}$=0.8	$\omega_{1,2}$=1.0 $\omega_{3,4}$=1.0
Supersonic, M = 1.65	374s	396s	395s	394s	393s	398s

10 Conclusion

The application of the artificial compression method of Harten to a density-based procedure blended with the Riemann solver was presented in this study. The method incorporated bounded high resolution of discontinuities. The boundedness criteria for this procedure were determined by using Jameson, TVD and ACM schemes that were applied to the fluxes of the convected quantities at the cell surfaces. A collocated finite volume method was used to solve the governing equations in a general coordinate system. The flux limiter and ACM switch were based on the characteristic variables. The main findings of the study can be summarized as follows:

1- By imposing ACM and TVD methods, the accuracy limitation of the density-based algorithm in the shock wave capturing was improved in the compressible regime.

2- The characteristics velocities are better converged due to the augmentation of the limiter. Therefore, with a same algorithm, the ACM and TVD methods captured the shock waves with higher resolution than the Jameson method. Shock waves include simple waves, reflected waves, and interaction of waves.

3- TVD method had a good quality in the shock wave capturing in comparison with the previously data obtained by density-based methods, while it had a less accuracy relative to the ACM.

4- In this work, not only quality of shock wave capturing was improved for all flows at the discontinuities by employing ACM and TVD methods, but also the computational time and convergence were improved for the supersonic flows.

5- In order to stabilize the solution convergence and improve the solution procedure for coarse grids, the ACM coefficients for nonlinear fields should be less than those of the linear fields. Hereby, sufficient numerical diffusion is provided for stability of solution. On the other hand, reduction of computational cells decreased the operations, thereby improving the convergence.

6- Convergence improvement should be considered in various aspects of this study, including calculation and decomposition agent vectors, agent values, and passing flux over oblique surfaces into the main coordinate.

References

[1] Harten, A., "High Resolution Scheme for Hyperbolic Conservation Laws", Journal of Computational Physics, Vol. 49, No. 3, pp. 357-393, (1983).

[2] Jameson, A., Schmidt, W., and Turkel, E., "Numerical Solutions of the Euler Equations by Finite-Volume Methods using Runge–kutta Time-stepping Schemes", AIAA, pp. 81-125, (1981).

[3] Harten, A., "The Artificial Compression Method for Computation of Shocks and Contact Discontinuities. I. Single Conservation Lows", Comm. Pure & Appl., pp. 611-637, (1977).

[4] Harten, A., "The Artificial Compression Method for Computation of Shocks and Contact Discontinuities: III. Self-Adjusting Hybrid Schemes", Math. Comput, Vol. 32, No. 142, pp. 363-389, (1978).

[5] Yee, H., Warming, R.F., and Harten, A., "Implicit Total Variation Diminishing (TVD) Schemes for Steady State Calculations", J. Comput. Phys, Vol. 57, No. 2, pp. 327-360, (1985).

[6] Yee, H.C., Sandham, N.D., and Djomeri, M.J., "Low Dissipative High-order Shock-Capturing Methods using Characteristic-Based Filters", J. Comput. Phys, Vol. 150, pp. 199-238, (1999).

[7] Lie, K.A., and Noelle, S., "On the Artificial Compression Method for Second-Order Non Oscillatory Central Difference Schemes for Systems of Conservation Laws", SIAM J. Sci. Comput, Vol. 24, No. 4, pp. 1157-1174, (2003).

[8] Yadegari, M., and Abdollahi Jahdi, M.H., "Shock Capturing Method by Numerical Dissipation Control on Symmetric Airfoil", Journal of Solid and Fluid Mechanics, Vol. 6, pp. 285-304, (2016).

[9] Lien, F.S., and Leschziner, M.A.," A Pressure–velocity Solution Strategy for Compressible Flow and Its Application to Shock Boundary Layer Interaction using Second-moment Turbulence Closure", J. Fluids Eng, Vol. 115, No. 4, pp. 717-725, (1993).

[10] Van Leer, B., "Towards the Ultimate Conservation Difference Scheme. II. Monotonicity and Conservation Combined in Second-order Scheme", J. Comput. Phys, Vol. 14, No. 4, pp. 361-370, (1974).

[11] Shyy, W., and Thakur, S., "Controlled Variation Scheme in a Sequential Solver for Recirculating Flows", Heat Transf, Vol. 25, pp. 273-286, (1994).

[12] Thakur, S., Wright, J., Shyy, W., Liu, J., Ouyang, H., and Vu, T., "Development of Pressure-based Composite Multigrid Methods for Complex Fluid Flows", Prog, Aerospace Sci, Vol. 32, No. 4, pp. 313-375, (1996).

[13] Mulder, W.A., and Van Leer, B., "Experiments with Implicit Upwind Methods for the Euler Equations", J. Comput. Phys, Vol. 59, pp. 232-246, (1985).

[14] Lin, H., and Chieng, C.C., "Characteristic-Based Flux Limiters of an Essentially Third-Order Flux-Splitting Method for Hyperbolic Conservation Laws", Int. J. Numer. Methods Fluids, Vol. 13, No. 3, pp. 287-307, (1991).

[15] Issa, R.I., and Javareshkian, M.H., "Application of TVD Schemes in Pressure-based Finite-volume Methods", In: Proceedings of the Fluids Engineering, (1996).

[16] Issa, R.I., and Javareshkian, M.H., "Pressure-based Compressible Calculation Method Utilizing Total Variation Diminishing Schemes", AIAA J. Vol. 36, No. 9, pp. 1652-1657, (1998).

[17] Kobayashi, M.H., and Pereira, J.C.F., "Characteristic-based Pressure Correction at All Speeds", AIAA J., Vol. 34, No. 2, pp. 272-280, (1996).

[18] Turkel, E., "Preconditioned Methods for Solving the Incompressible and Low Speed Compressible Equations", J. Comput. Phys, Vol. 72, pp. 277-298, (1987).

[19] Turkel, E., Radespiel, R., and Kroll, N., "Assessment of Preconditioning Methods for Multidimensional Aerodynamics", Comp. Fluids, Vol. 26, No. 6, pp. 613-634, (1997).

[20] Guillard, H., and Viozat, C., "On the Behavior of Upwind Schemes in the Low Mach Number Limit", Comp. Fluids, Vol. 28, No. 1, pp. 63-86, (1999).

[21] Zamzamian, K., and Razavi, S.E., "Multidimensional Upwinding for Incompressible Flows Based on Characteristics", J. Comput. Phys, Vol. 227, No. 19, pp. 8699-8713, (2008).

[22] Godunov, S. K.A., "Difference Scheme for Numerical Computation of Discontinuous Solutions of Hydrodynamic Equations", MathSbornic, English Translation in U.Sjointpublications, Vol . 47, pp. 271-306, (1959).

[23] Roe, P. L., "Approximate Riemann Solvers, Parameter Vectors and Difference Schemes", Journal of Computational Physics, Vol. 43, pp. 357-372, (1981).

[24] Colella, P., and Woodward, P. R., "The Piecewise Parabolic Method (PPM) for Gas Dynamical Simulations", J. of Comput. Phys, Vol. 54, pp. 174-201, (1984).

Nomenclature

c_v	The specific heat at constant volume(m^2/s^2.K)
E	Internal energy (kg. m^2/s^2)
$\vec{f}_e$	External forces (kg.m/s^2)
$\vec{F}$	The flux vector
g_i^l	The limited function
H	The total enthalpy of the fluid (kg. m^2/s^2)
$\bar{I}$	The unit matrix
$\hat{k}_x$	The Cartesian components of unit vector of $\vec{k}$
$\hat{k}_y$	The Cartesian components of unit vector of $\vec{k}$
k	Coefficient
M	Mach number
P	Pressure (kg/ms^2)
u	The velocity components of $\vec{v}$ in x direction (m/s)
v	The velocity components of $\vec{v}$ in y direction (m/s)
$\vec{v}$	The velocity vector (m/s)
α	The characteristic variable
α_e^l	The characteristic variable at the e surface of the cell
$\lambda_e^l\ i$	The value of the l[th] characteristic at the e surface of the cell
λ_i	The agents value
ρ	Density (kg/m^3)
Γ	Area (m^2)
$\emptyset_i^l$	The anti-diffusion function at the surface of the i[th] cell
ψ	The enthalpy function
ω	The coefficient of ACM
Ω	Volume (m^3)